Coupled Target - Blanket Neutronics and Photonics Analysis for the University of Wisconsin Heavy Ion Beam Fusion Reactor Design

M.E. Sawan, W.F. Vogelsang, and G.A. Moses

November 1980

UWFDM-395

Trans. ANS 38 (1981) 574.

FUSION TECHNOLOGY INSTITUTE

UNIVERSITY OF WISCONSIN

MADISON WISCONSIN

Coupled Target - Blanket Neutronics and Photonics Analysis for the University of Wisconsin Heavy Ion Beam Fusion Reactor Design

M.E. Sawan, W.F. Vogelsang, and G.A. Moses

Fusion Technology Institute
University of Wisconsin
1500 Engineering Drive
Madison, WI 53706

http://fti.neep.wisc.edu

November 1980

UWFDM-395

Trans. ANS 38 (1981) 574.

Coupled Target - Blanket Neutronics and Photonics Analysis for the University of Wisconsin Heavy Ion Beam Fusion Reactor Design

Mohamed E. Sawan

William F. Vogelsang

Gregory A. Moses

Fusion Engineering Program

Nuclear Engineering Department

University of Wisconsin

Madison, Wisconsin 53706

November 1980

UWFDM-395

Abstract

Consistent coupled target - blanket neutronics and photonics calculations are performed for the University of Wisconsin heavy ion beam fusion reactor conceptual design. Neutron target interactions leading to neutron multiplication, spectrum softening, and gamma production are considered. The tritium breeding ratio is found to be 1.175. An overall energy multiplication of 1.24 is found to be achieved in the system. The effect of the blanket "effective thickness" on the different reactor parameters is investigated. The effect of neglecting neutron target interactions is also investigated.

I. Introduction

Neutronics and photonics calculations are required to determine important fusion reactor parameters such as tritium breeding, nuclear heating, and radiation damage. No neutron fuel interactions occur in the low density plasma of a magnetic confinement fusion reactor. In an inertial confinement fusion reactor, the DT fuel is heated and compressed to extremely high densities before it ignites. Therefore, neutron fuel interactions cannot be neglected in an inertial confinement fusion reactor. The spectrum of emerging neutrons softens as a result of elastic and inelastic collisions with the target constituent materials and neutron multiplication occurs as a result of (n,2n) and (n,3n) reactions. This affects the performance of the blanket, first wall, reflector and shield. Neutron fuel interactions produce gamma photons which contribute to nuclear heating in the blanket. A consistent neutronics and photonics analysis must, therefore, account for neutron target interactions. This is done by performing detailed neutronics and photonics calculations within the pellet and coupling them to the blanket calculations. Most previous models for inertial confinement systems have neglected neutron fuel interactions and used a pure 14.1 MeV neutron source.[1,2]

A new approach to inertial confinement fusion that is drawing increasing attention is the use of accelerated heavy ions as a fusion pellet driver. The interaction of heavy ion beams (HIB) with matter is thought to be better understood than the interaction of laser or electron beams with matter. Furthermore, the coupling efficiency of heavy ions with the fusion pellet is higher than that for photons or electrons.[3] In addition, heavy ion accelerators have higher efficiencies and greater reliability than large laser systems. Another advantage of the heavy ion beam fusion reactor concept is

the possibility of attaining high pulse repetition rate without a severe penalty in capital investment.[4]

In this work a consistent coupled target-blanket neutronics and photonics study is given for the University of Wisconsin HIB fusion reactor conceptual design. The effect of neglecting neutron pellet interactions on the different reactor parameters is investigated. The reactor design uses $Li_{17}Pb_{83}$ liquid metal eutectic as the coolant/breeder and for protecting the first wall. Among LiPb alloys, $Li_{17}Pb_{83}$ is chosen because it has the lowest melting point (500 K) and the least reactivity with water.[5] For further understanding of the neutronics and photonics characteristics of $Li_{17}Pb_{83}$, the effect of the effective coolant thickness on the neutronic and photonic dependent parameters of the system is investigated.

II. HIB Target Model

The target used in the University of Wisconsin HIB fusion reactor design is similar to that reported by Bangerter and Meeker[6] with the TaCOH pusher replaced by a mixture of 93.25 wt% Li and 6.75 wt% Pb which has the same density as the TaCOH pusher. The high Z material (Pb) used in the pusher inhibits energy transport into the fuel and prevents preheating. The low density of the pusher helps avoid the problem of fluid instabilities because of the small density difference between the pusher and the fuel. The target design used includes a high density Pb tamper which acts as a confinement shell to increase the efficiency of implosion.

The energy input to the pellet by 10 GeV Bi^{++} ions is accumulated over an implosion time of 40 ns and concentrated in the fuel resulting in ignition at the end of this period. At ignition the DT fuel is assumed to have a ρR value of 2 g/cm^2. This corresponds to a density which is 872 times the solid fuel density. The pusher is assumed to be compressed to the same density as the

fuel with a ρR value of 1 g/cm^2. The configuration of the pellet initially and at ignition is illustrated in Fig. 1.

Detailed neutronics and photonics calculations are performed within the pellet at ignition. The multi-group discrete ordinates code ANISN[7] is used yielding time integrated results. An isotropic source of 14.1 MeV neutrons is distributed uniformly in the DT fuel region. A coupled 25 neutron - 21 gamma group cross section library is used throughout this work. The library consists of the RSIC DLC-41B/VITAMIN-C data library[8] and the DLC-60/MACKLIB-IV response data library.[9]

Table 1 lists the density data for the final pellet state used in this work. The target design used in the neutronics and photonics calculations utilizes 1 mg of DT fuel (same as the design in ref. 6) which produces an energy yield of 100 MJ per shot. Since a DT energy yield of 400 MJ is proposed for the University of Wisconsin HIB fusion reactor design, the results are scaled by a factor of 4. Assuming that the ρR values for the 100 MJ and 400 MJ targets are the same, the neutron and gamma spectra obtained for the 100 MJ yield case can be used for a yield of 400 MJ. The results presented here are based on a DT yield of 400 MJ and a repetition rate of 5 Hz yielding 7.1 x 10^{20} fusion neutrons per second.

III. HIB Reactor Model

The HIB fusion reactor power plant design incorporates four cylindrical cavities each having a radius of 7 m and a height of 10 m. The blanket region consists of an array of porous tubes made of braided SiC through which the $Li_{17}Pb_{83}$ liquid metal eutectic flows. These tubes are placed inside the reactor cavity. Besides serving as the coolant and tritium breeder, the $Li_{17}Pb_{83}$ coolant is utilized for first wall protection. The tubes occupy 30% of the 2 m thick blanket region yielding an effective blanket thickness of 60

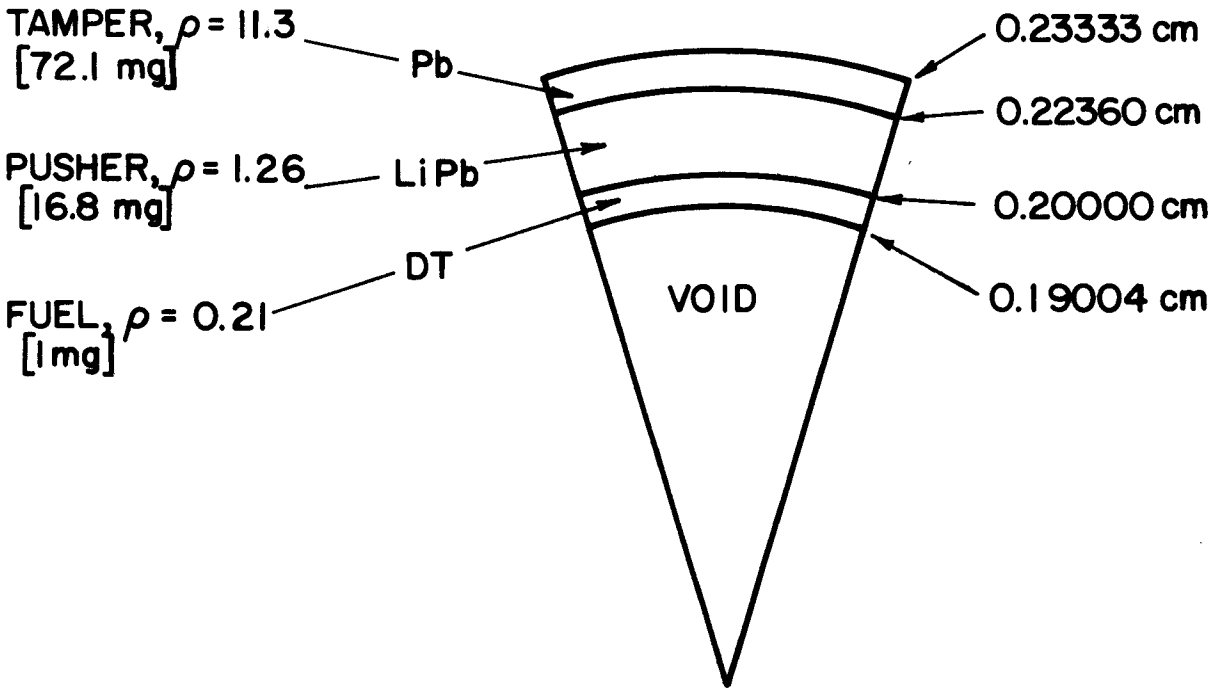

INITIAL TARGET STATE

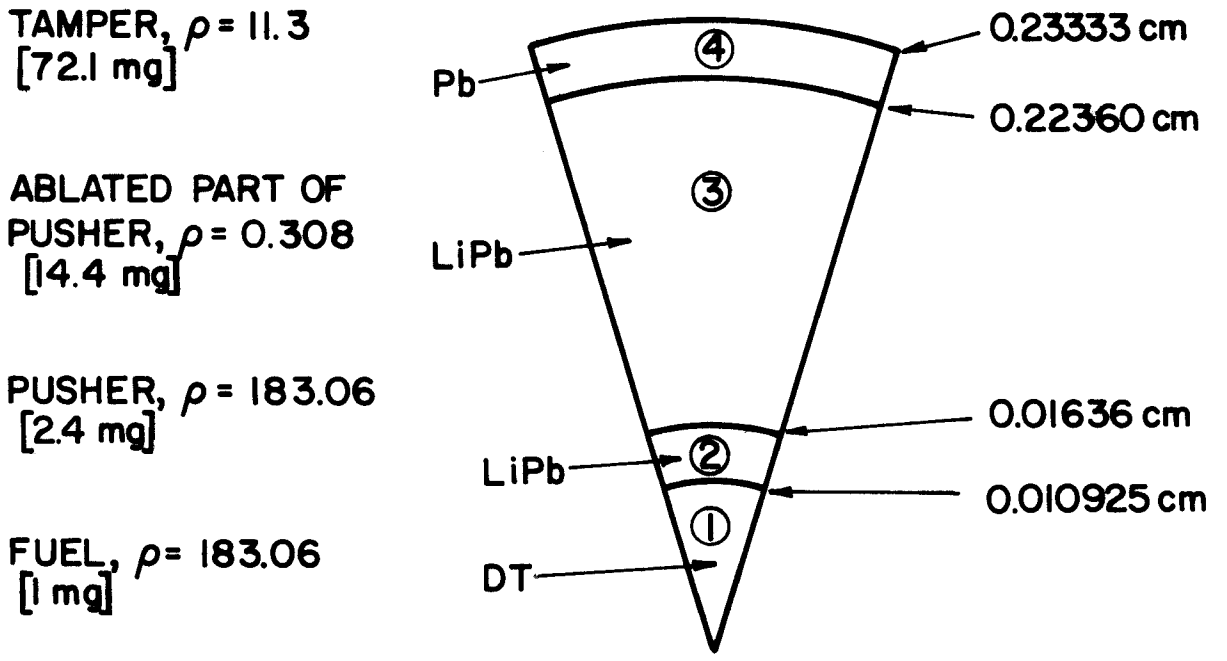

FINAL TARGET STATE

Figure 1 HIB pellet model.

Table 1. Pellet Data at Ignition

Region	Composition	Density [g/cm^3]	ρR [g/cm^2]	Atomic Density [atoms/b cm]
1	D	183.06	2	22.225
	T			22.225
2	^6Li	183.06	1	0.4656
	^7Li			5.809
	Pb			0.32166
3	^6Li	0.308	0.0638	7.834×10^{-4}
	^7Li			9.774×10^{-3}
	Pb			5.412×10^{-4}
4	Pb	11.3	0.11	3.2831×10^{-2}

cm. The LiPb coolant occupies 80% of the tube volume with the SiC structural material occupying the remaining 20%. SiC and $Li_{17}Pb_{83}$ have nominal densities of 3.17 and 9.4 g/cm^3, respectively. The first wall is made of ferritic steel (HT-9) which is an alloy composed of 85.25 wt% iron and 11.5 wt% chromium. The first wall has a thickness of 1 cm and a density of 7.8 g/cm^3. A 0.4 m thick reflector composed of 90 v/o ferritic steel structure and 10 v/o $Li_{17}Pb_{83}$ coolant is used. The reactor utilizes a 3.5 m thick concrete shield. The shield is not included in the neutronics calculations presented here and appropriate albedos are used to account for possible backscattering from the shield. A schematic of the blanket, first wall, reflector, and shield configuration for the HIB fusion reactor is given in Fig. 2. The nuclide densities used in the calculations are given in Table 2.

The code ANISN is used to perform neutronics and photonics calculations yielding average time integrated results. A spherical geometry is used in the calculations and hence the results represent the worst conditions at the central plane of the reactor. The results give conservatively high damage rates and low tritium breeding ratios. The neutron and gamma spectra obtained from the target calculations are used to represent the source for the blanket neutronics and photonics calculations. The source is considered to be an isotropic point source at the center of the cavity. The calculations account for neutron spectrum softening, neutron multiplication, and gamma production in the pellet. The results are compared to the results obtained using a 14.1 MeV neutron source with no account taken for neutron pellet interactions. The effect of blanket "effective thickness" on radiation damage, tritium breeding, and nuclear heating is also investigated.

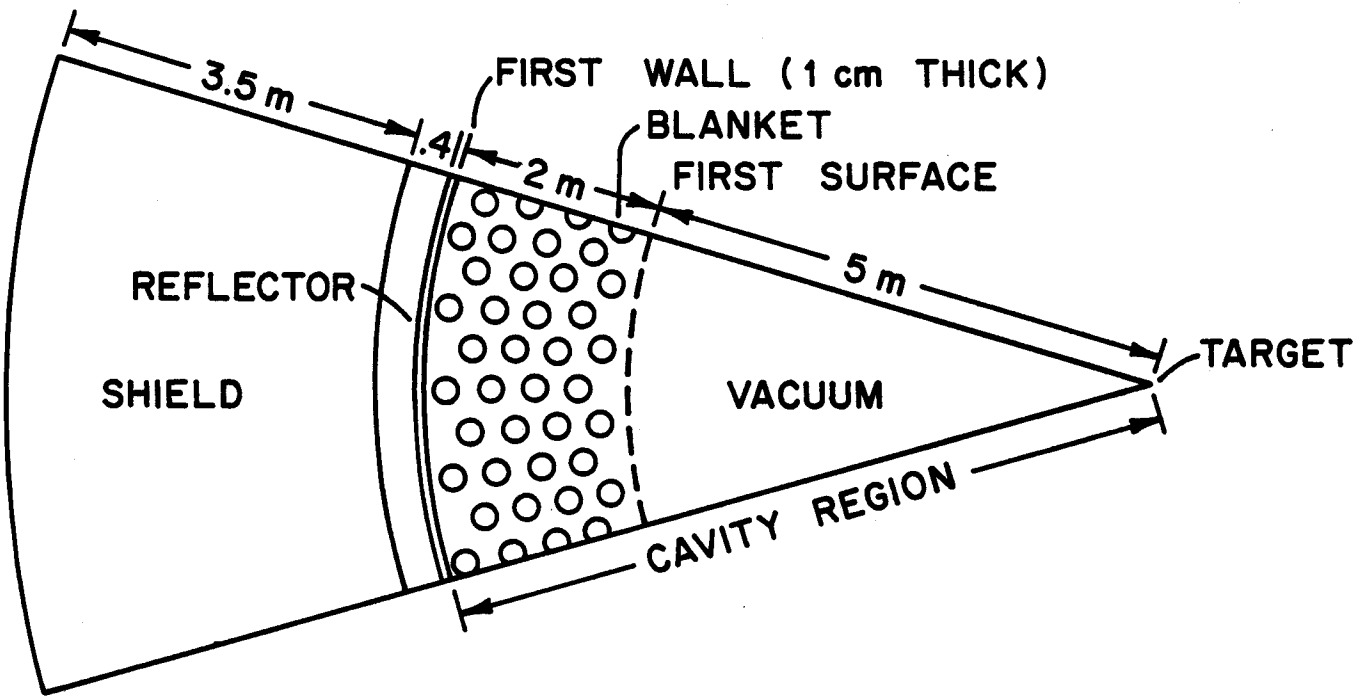

Figure 2 HIB reactor cavity model.

Table 2

Nuclide Densities Used in Neutronics Analysis of HIB Fusion Reactor

Region	Constituent Elements	Nuclide Density (nuclei/b cm)
Blanket	^{6}Li	.00033
[80 v/o $Li_{17}Pb_{83}$	^{7}Li	.00412
+ 20 v/o SiC]	Si	.00953
(.3 density factor)	C	.00953
	Pb	.02172
Ferritic Steel	Fe	.07174
First Wall	Cr	.01725
(1.0 density factor)	Ni	.00066
	Mo	.00081
	V	.00046
	Si	.00069
	Mn	.00071
	C	.00130
	W	.00022
Reflector	Fe	.06456
[90 v/o ferritic	Cr	.01553
steel + 10 v/o $Li_{17}Pb_{83}$]	Ni	.00060
(1.0 density factor)	Mo	.00073
	V	.00041
	Si	.00063
	Mn	.00064
	C	.00117
	W	.00020
	^{6}Li	.00004
	^{7}Li	.00051
	Pb	.00272

IV. Neutron and Gamma Spectra

The calculated spectrum of neutrons escaping from the target, which represents the neutron source for the blanket calculations, is given in Fig. 3. The large peak at 14.1 MeV is due to the uncollided flux of neutrons escaping the target. This amounts to 70.75% of neutrons leaking from the target. Local peaking of the flux at 2 and 4 MeV is caused by backward elastic scattering of 14.1 MeV neutrons with D and T, respectively. The lower energy range contains neutrons that have been elastically and inelastically scattered and those produced by (n,2n) and (n,3n) reactions. The average energy of emerging neutrons is 11.98 MeV. The results show that a pellet neutron multiplication of 1.046 is obtained. This results mainly from (n,2n) reactions in the dense DT fuel and LiPb pusher. The (n,2n) and (n,3n) reactions per fusion are given in Table 3 for the different target regions.

The spectrum of gamma rays leaking from the target is given in Fig. 4. The spectrum peaks around .6 MeV. The average energy of the gamma photons emerging from the target is 1.533 MeV.

Using the neutron and gamma spectra from the target calculations to represent the source for the blanket neutronics and photonics calculations, the neutron and gamma spectra are calculated at different positions in the blanket, first wall and reflector. The neutron spectra are given in Fig. 5. In the innermost part of the blanket the spectrum has a pronounced peak at 14.1 MeV with the lower energy part of the spectrum resulting from neutron pellet interactions and neutron slowing down in the blanket itself. In the first wall and reflector the spectrum is considerably softened primarily because of slowing down in the blanket - reflector system.

In Fig. 6 the gamma spectra in the first wall and the center of the blanket are compared. The gamma photon density in the first wall is larger

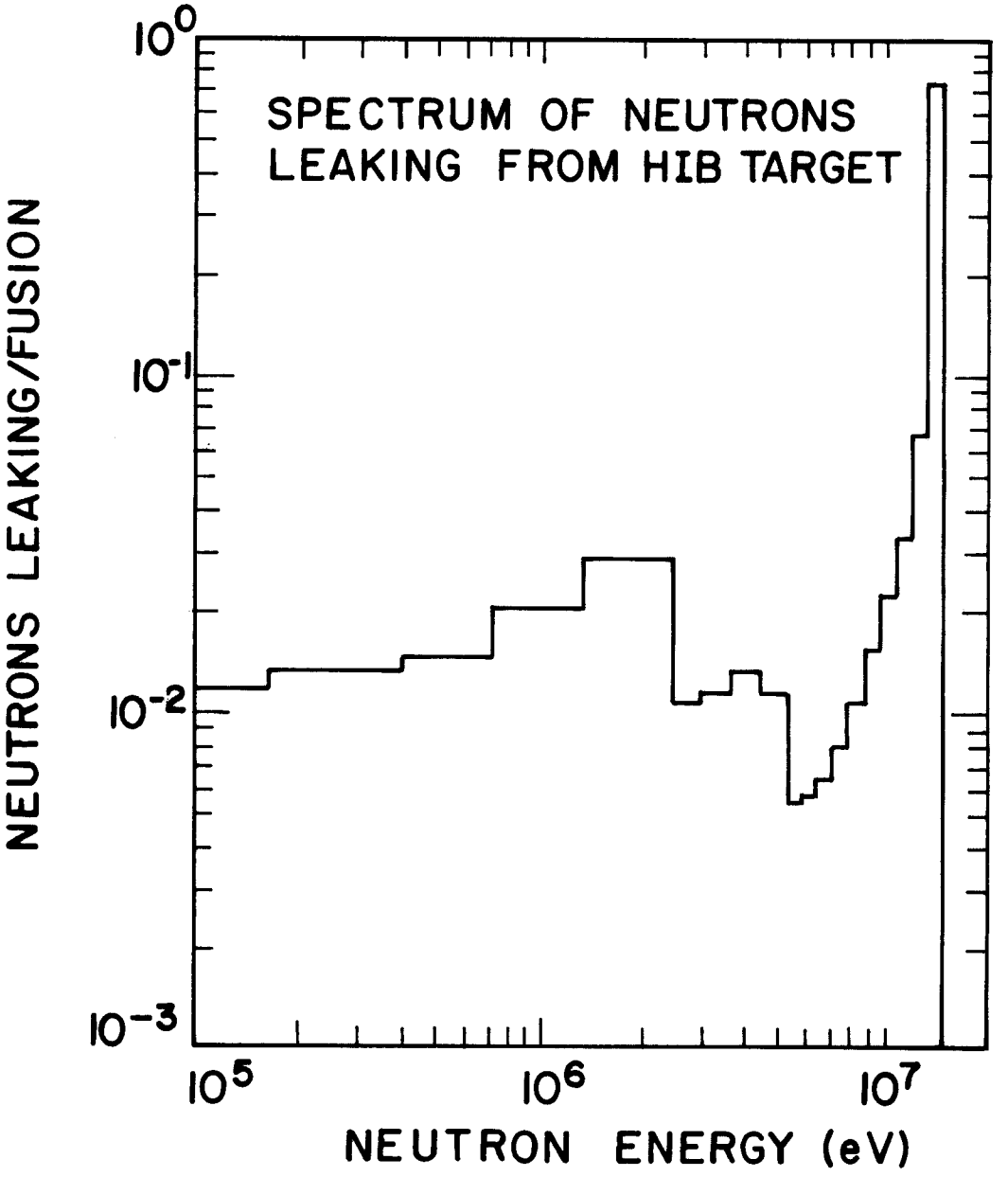

Figure 3 Spectrum of neutrons leaking from the target.

Table 3. [n,2n] and [n,3n] Reactions in the Target

Region	Reactions/Fusion	
	[n,2n]	[n,3n]
1	4.04323×10^{-2}	0.0
2	5.09718×10^{-3}	5.63702×10^{-5}
3	3.64793×10^{-4}	4.00264×10^{-6}
4	6.63362×10^{-4}	8.59598×10^{-6}
Total	4.65576×10^{-2}	6.89688×10^{-5}

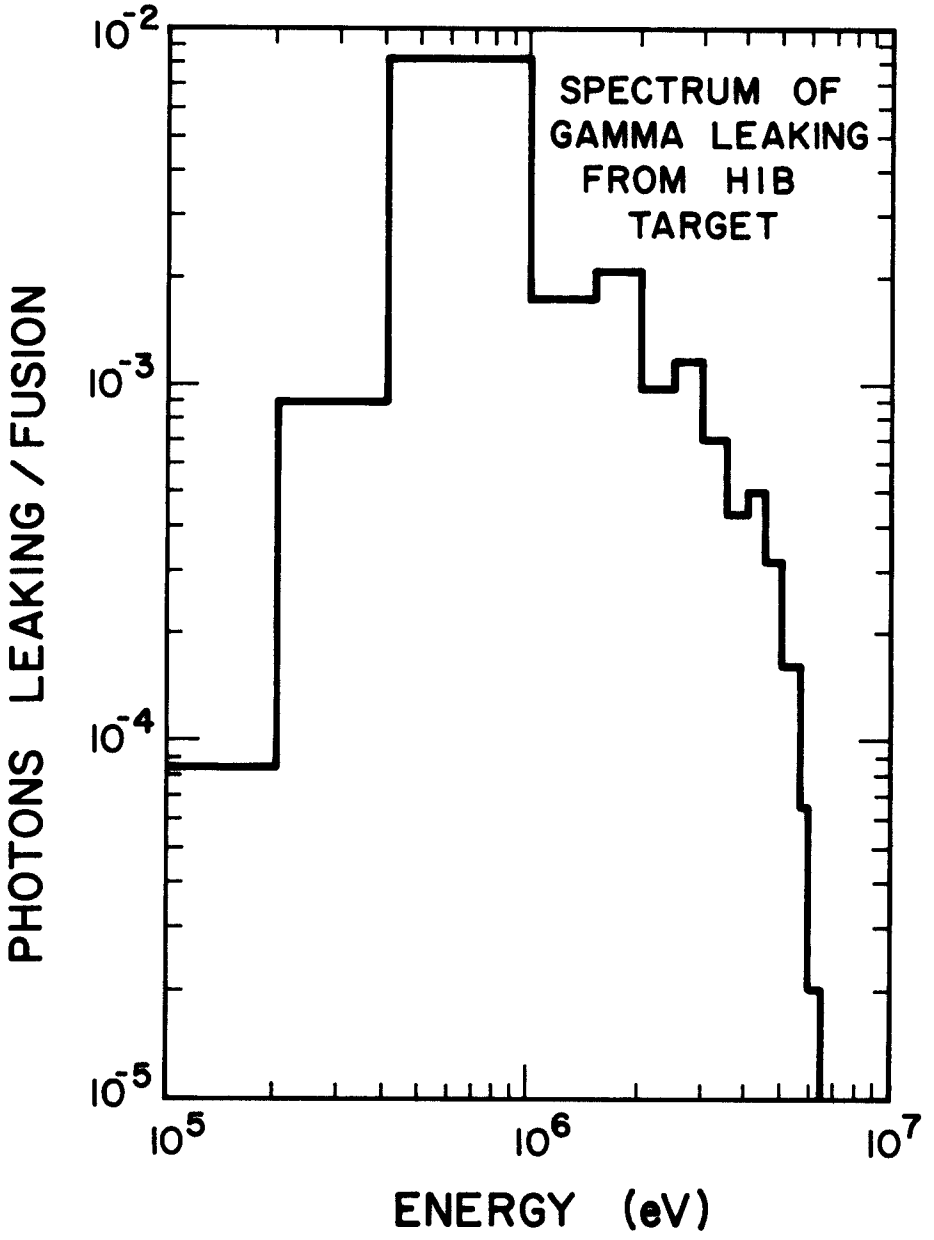

Figure 4 Spectrum of gammas leaking from the target.

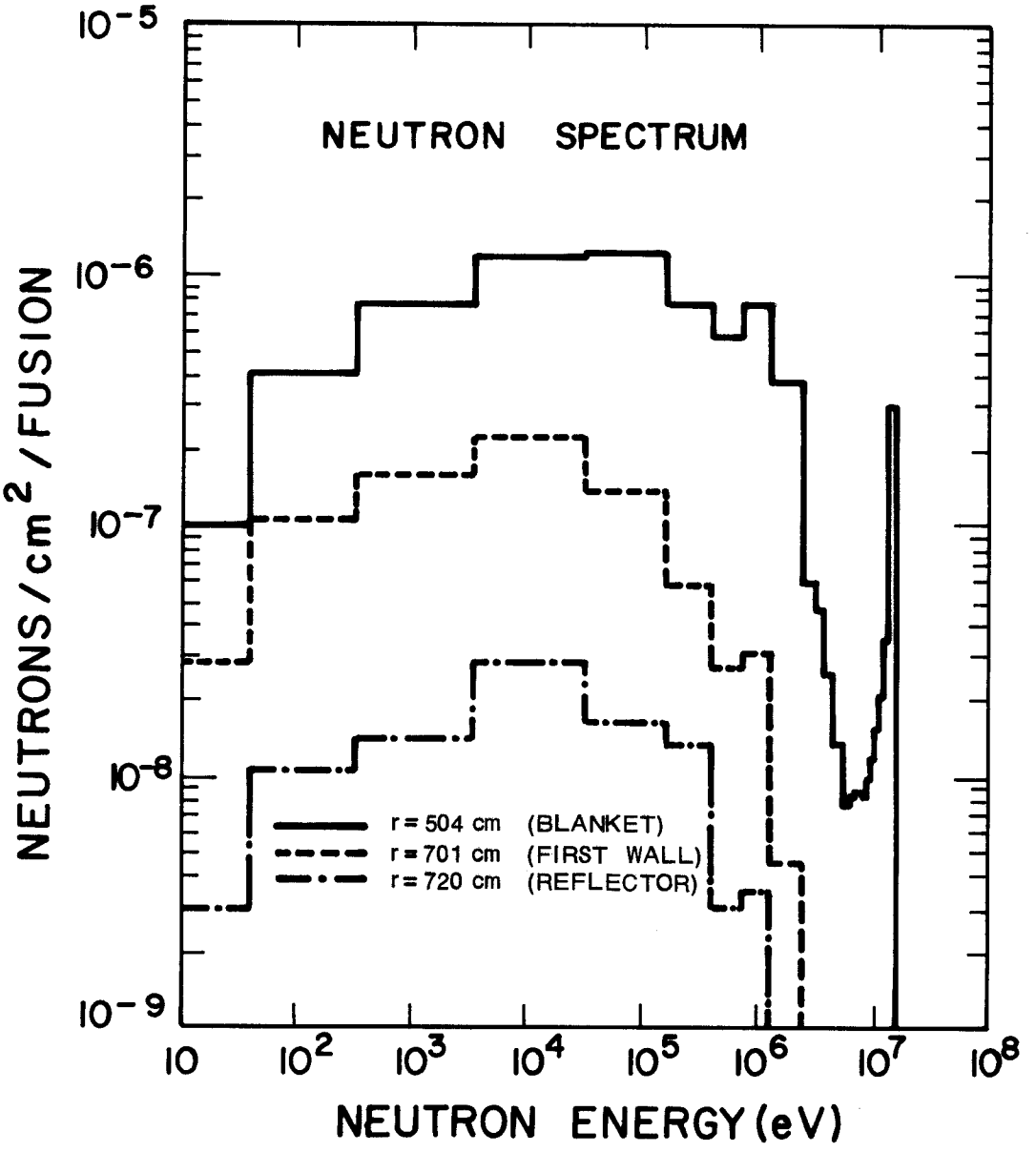

Figure 5 Neutron spectrum in the blanket, first wall, and reflector.

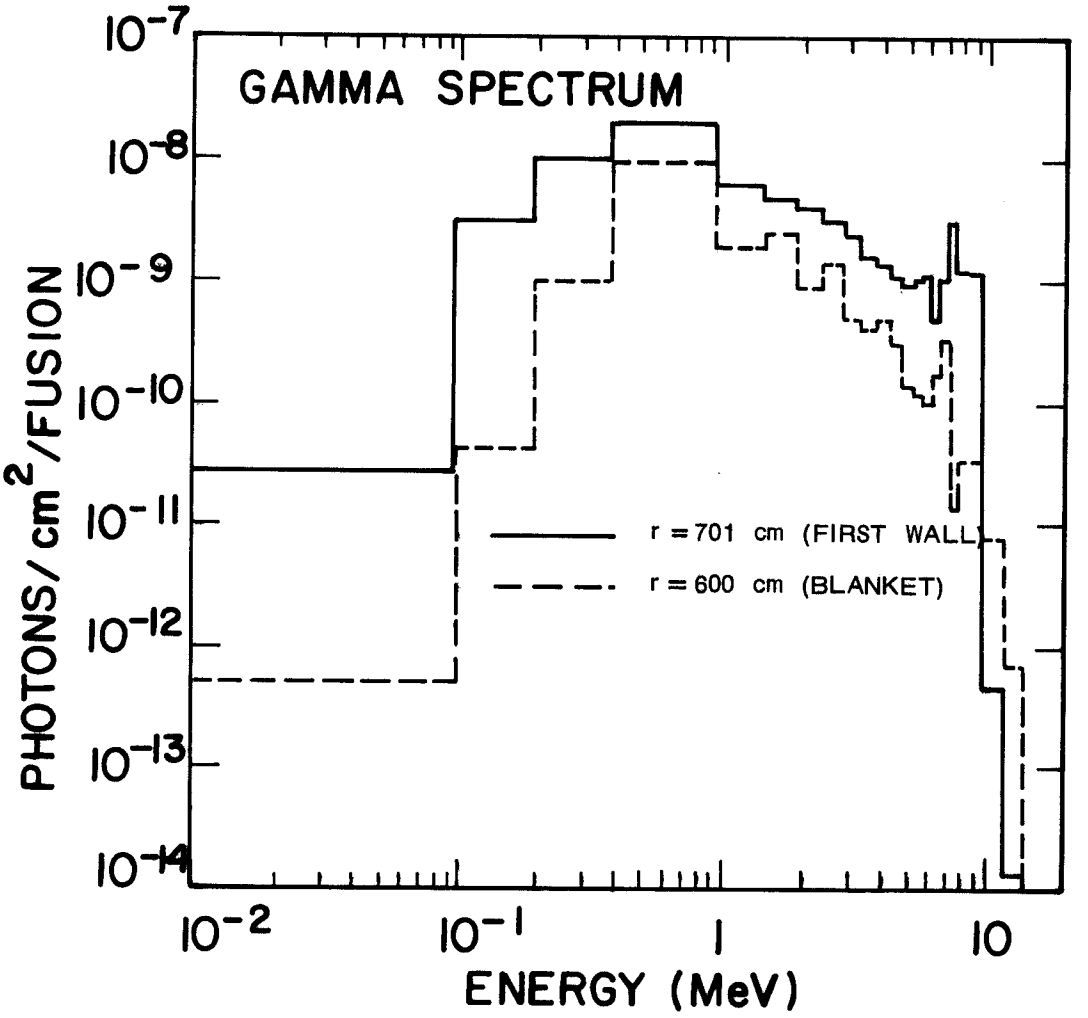

Figure 6 Gamma spectrum in the blanket and first wall.

than that in the blanket because of the large gamma production cross section in iron.

V. Tritium Production

Neutron interactions with Li used in the target are found to produce .0146 tritium atoms per DT fusion reaction. Most of this tritium is produced in ^{7}Li because of the relatively hard spectrum of neutrons in the target. Tritium production in the target is very small compared to that in the blanket.

Fig. 7 gives the spatial distribution of tritium production in the blanket and reflector. The contributions to tritium production from ^{7}Li and ^{6}Li are shown. The contribution from ^{7}Li, which is a high energy reaction (threshold energy = 2.86 MeV), decreases sharply as one moves into the blanket away from the source because of the increased softening of the spectrum. A breeding ratio of 1.175 is obtained.

Table 4 gives the effect of blanket thickness and neutron pellet interactions on tritium production. It is clear that tritium production in the blanket increases as the thickness increases. On the other hand, tritium production in the reflector region decreases as the blanket thickness increases. The net effect is that the overall breeding ratio increases nearly linearly with the blanket thickness. The results show that neglecting neutron target interactions tends to overestimate the tritium breeding ratio. We notice that both the contributions from ^{6}Li and ^{7}Li increase if one uses a 14.1 MeV neutron source. The contribution from ^{7}Li increases because of the larger neutron flux at 14.1 MeV. The contribution from ^{6}Li increases because more (n,2n) reactions occur in lead resulting in a larger neutron flux at low energies where the $^{6}Li(n,\alpha)T$ reaction cross section is large.

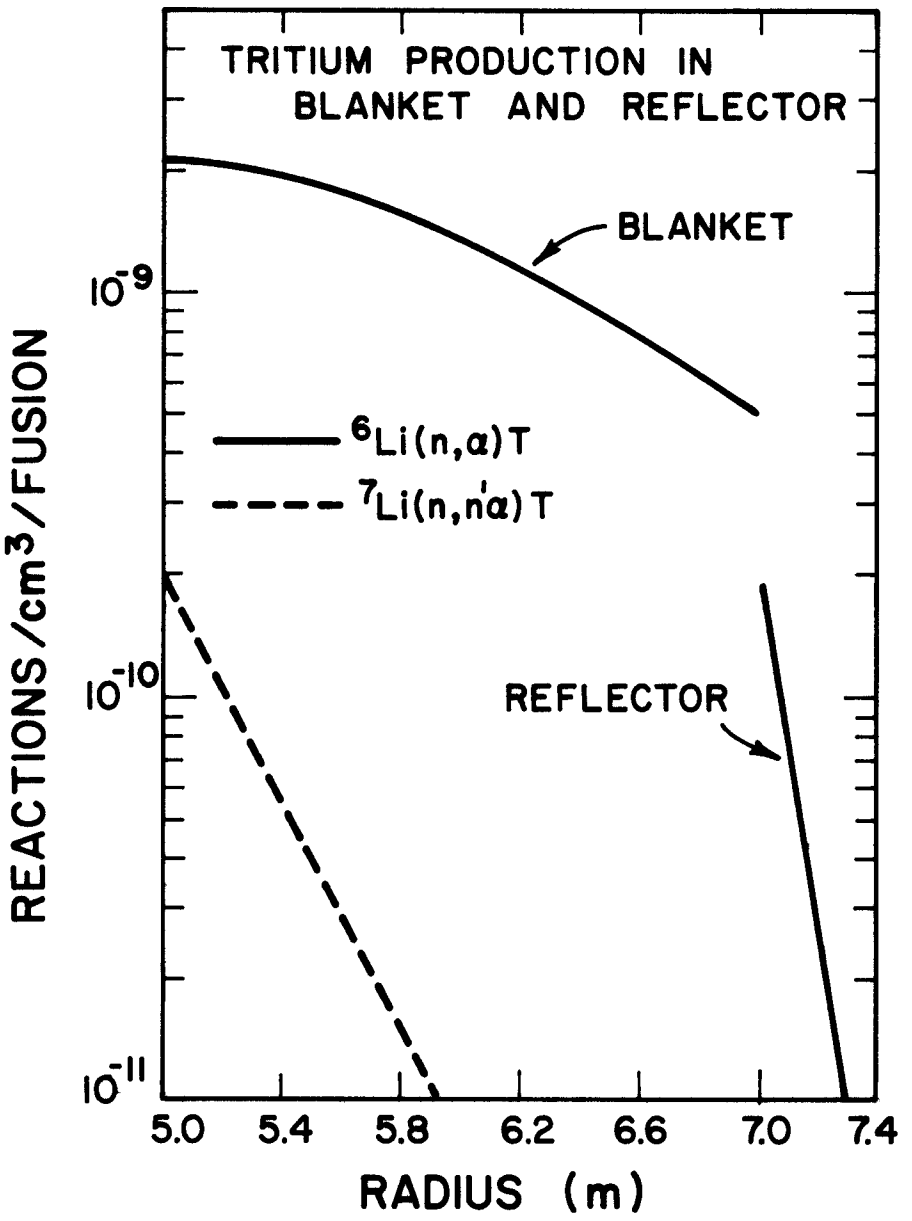

Figure 7 Tritium production in the blanket and reflector.

Table 4

Effect of Blanket Thickness and Target Interactions on Tritium Production (Tritons/Fusion)

		Neutron Target Interactions Included				14.1 MeV Source
Effective Blanket Thickness (cm)		0	25	50	60	60
Region						
Blanket	$^{6}Li(n,\alpha)T$	------	.47953	.99927	1.14118	1.17124
	$^{7}Li(n,n'\alpha)T$	------	.01988	.02183	.02196	.02392
	Subtotal	------	.49941	1.02110	1.16314	1.19516
Reflector	$^{6}Li(n,\alpha)T$	.04124	.03589	.01740	.01209	.01262
	$^{7}Li(n,n'\alpha)T$	.00141	.00014	.00001	.00001	.00001
	Subtotal	.04265	.03603	.01741	0.01210	.01263
System Total		.04265	.53544	1.03851	1.17524	1.20779

VI. Radiation Damage to Structural Materials

The effects of blanket thickness and neutron target interactions on the maximum atomic displacements per full power year in SiC structural material of the blanket, the first wall, and the structural material of the reflector are given in Table 5. The average dpa rate in the SiC tubes increases slightly as the blanket thickness increases while the dpa rates in ferritic steel first wall and structural material of the reflector decrease as the blanket thickness increases. The reason is that the dpa cross section for iron peaks at 14.1 MeV and has a threshold energy of ~ 1 keV with the total dpa in iron decreasing as the spectrum becomes softer. On the other hand, the dpa cross section for ^{12}C peaks at ~ 3.5 MeV and has a lower threshold energy of ~ .2 keV resulting in an increase in the total dpa in C as the spectrum softens. Neglecting neutron target interactions tends to overestimate the dpa rate in the first wall and structural material of the reflector and to underestimate the dpa rate in SiC structural material of the blanket. The reason is that using a 14.1 MeV neutron source results in a larger neutron flux at 14.1 MeV where the dpa cross section for iron peaks and a smaller neutron flux at ~ 3.5 MeV where the dpa cross section for ^{12}C peaks.

The helium and hydrogen gas production rates in the different structural materials are given in Table 6 for effective blanket thicknesses of 0, 25, 50, and 60 cm and for the case when neutron target interactions are neglected. The average gas production rate is found to decrease as the blanket thickness increases with the effect being more pronounced in the reflector and first wall. The reason is that the hydrogen and helium production cross sections peak at 14.1 MeV for SiC and ferritic steel. Furthermore, the reactions resulting in helium and hydrogen production are of a threshold nature with threshold energies in the low MeV energy range. The effect on gas production

Table 5

Effect of Blanket Thickness and Target

Interactions on Maximum Atomic Displacement (dpa/year)*

	Neutron Target Interactions Included				14.1 MeV Source
Effective Blanket Thickness (cm)	0	25	50	60	60
Region					
Structural Material in Blanket (SiC)	-	71.27	83.48	90.22	88.17
Ferritic Steel First Wall	25.360	9.078	2.570	1.500	1.590
Structural Material in Reflector (Ferritic Steel)	22.720	8.183	2.306	1.350	1.426

*Based on 400 MJ DT yield and a repetition rate of 5 Hz

Table 6

Effect of Blanket Thickness and Target Interactions on Maximum Gas Production (appm/year)*

	Neutron Target Interactions Included				14.1 MeV Source
Effective Blanket Thickness (cm)	0	25	50	60	60
Region					
	Helium Production				
Structural Material in Blanket (SiC)	-	4107.7	4036.0	4000.1	4800.1
Ferritic Steel First Wall	229.10	18.65	1.55	.57	.69
Structural Material in Reflector (Ferritic Steel)	186.10	15.68	1.29	.47	.57
	Hydrogen Production				
Structural Material in Blanket (SiC)	-	1560.0	1538.6	1527.0	1773.7
Ferritic Steel First Wall	736.93	63.87	5.53	2.07	2.47
Structural Material in Reflector (Ferritic Steel)	605.04	53.91	4.64	1.72	2.07

* Based on 400 MJ DT yield and a repetition rate of 5 Hz

is more pronounced than the effect on dpa because of the lower dpa threshold energy. Neglecting neutron target interactions is found to overestimate the gas production in the structural materials of the blanket - reflector system because of the larger neutron density at 14.1 MeV.

VII. Nuclear Energy Deposition

Neutron and gamma energy deposition in the target, blanket, first wall, and reflector are calculated using the neutron and gamma spectra and the appropriate kerma factors. Table 7 gives neutron and gamma energy deposition in the different regions of the target. Most of this energy is deposited by neutrons in the DT fuel core. The energy deposited in the target by neutrons and gamma photons is 1.263 MeV per fusion. When the 3.5 MeV energy carried by the alpha particle emerging from the fusion reaction is added, a total energy of 4.763 MeV per fusion is found to be carried by X-rays and pellet debris following the pellet microexplosion. The energy carried by emerging neutrons is found to be 12.532 MeV per fusion and the energy carried by gamma photons is found to be .027 MeV/fusion. The remaining energy of .278 MeV/fusion is lost in endoergic neutron reactions with the target materials.

The spatial variation of the neutron and gamma heating in the blanket and reflector is given in Fig. 8. Neutron energy deposition is found to decrease as one moves away from the source because of the increased neutron attenuation. Gamma heating decreases sharply in the blanket as one moves away from the source because of the large attenuation of gamma photons in lead. The large gamma production in iron causes the gamma heating to increase sharply as one approaches the first wall. The spatial variation of the total power density in the blanket is given in Fig. 9.

Table 8 gives the neutron, gamma, and total energy deposition in the different regions for different effective blanket thicknesses and for the case

Table 7 Neutron and Gamma Energy Deposition in the Target

Region	Element	Neutron Heating [eV/fusion]	Gamma Heating [eV/fusion]
1	DT	1.068×10^{6}	0.0
2	^{6}Li	1.70129×10^{4}	2.07881×10
	^{7}Li	1.62950×10^{5}	2.5936×10^{2}
	Pb	6.1056×10^{2}	9.06526×10^{2}
	Region Total	1.805734×10^{5}	1.18667×10^{3}
3	^{6}Li	1.20695×10^{3}	1.26611×10^{0}
	^{7}Li	1.16287×10^{4}	1.57965×10
	Pb	4.35637×10	5.4128×10
	Region Total	1.2879214×10^{4}	71.19061
4	Pb	9.38872×10	1.53527×10^{2}
Total		1.2615×10^{6}	1.14114×10^{3}

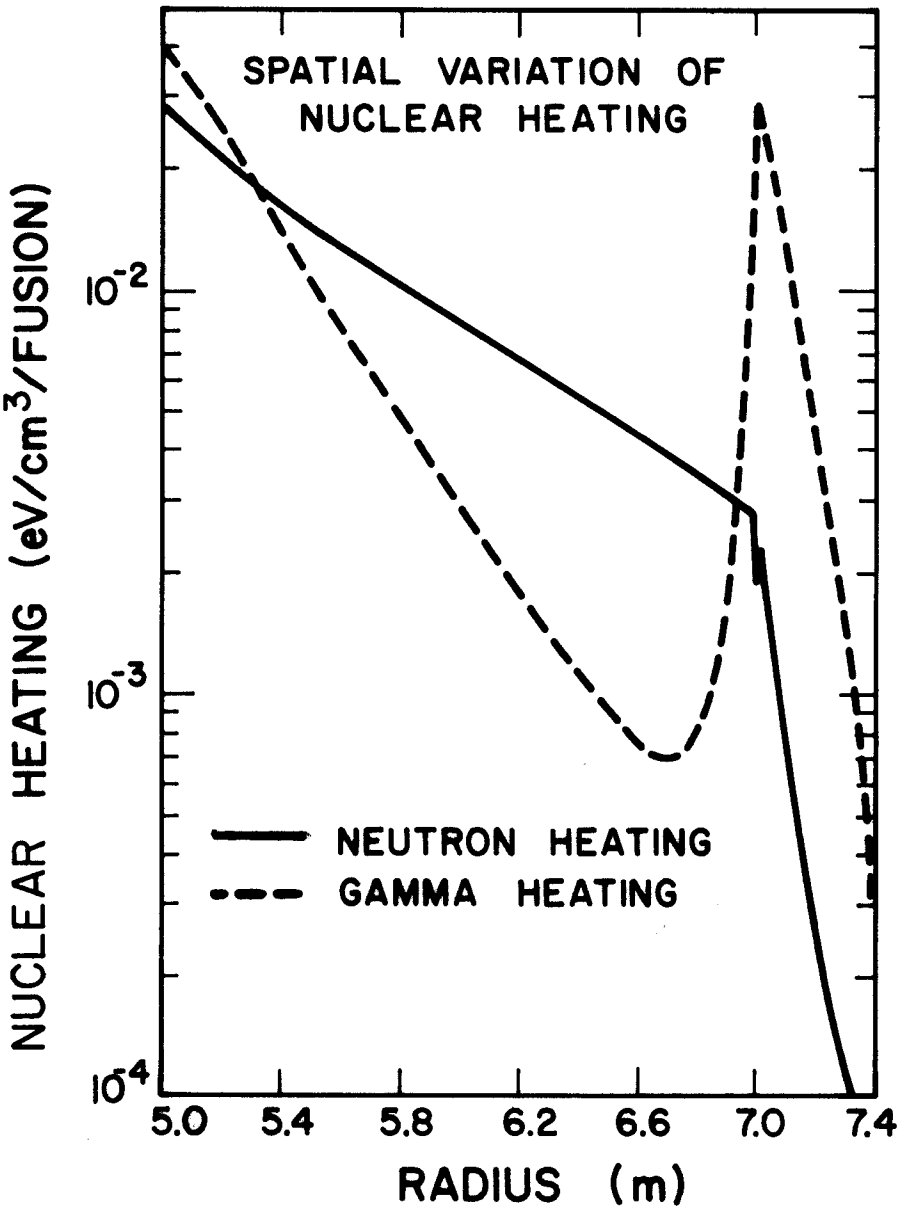

Figure 8 Spatial variation of nuclear heating in the system.

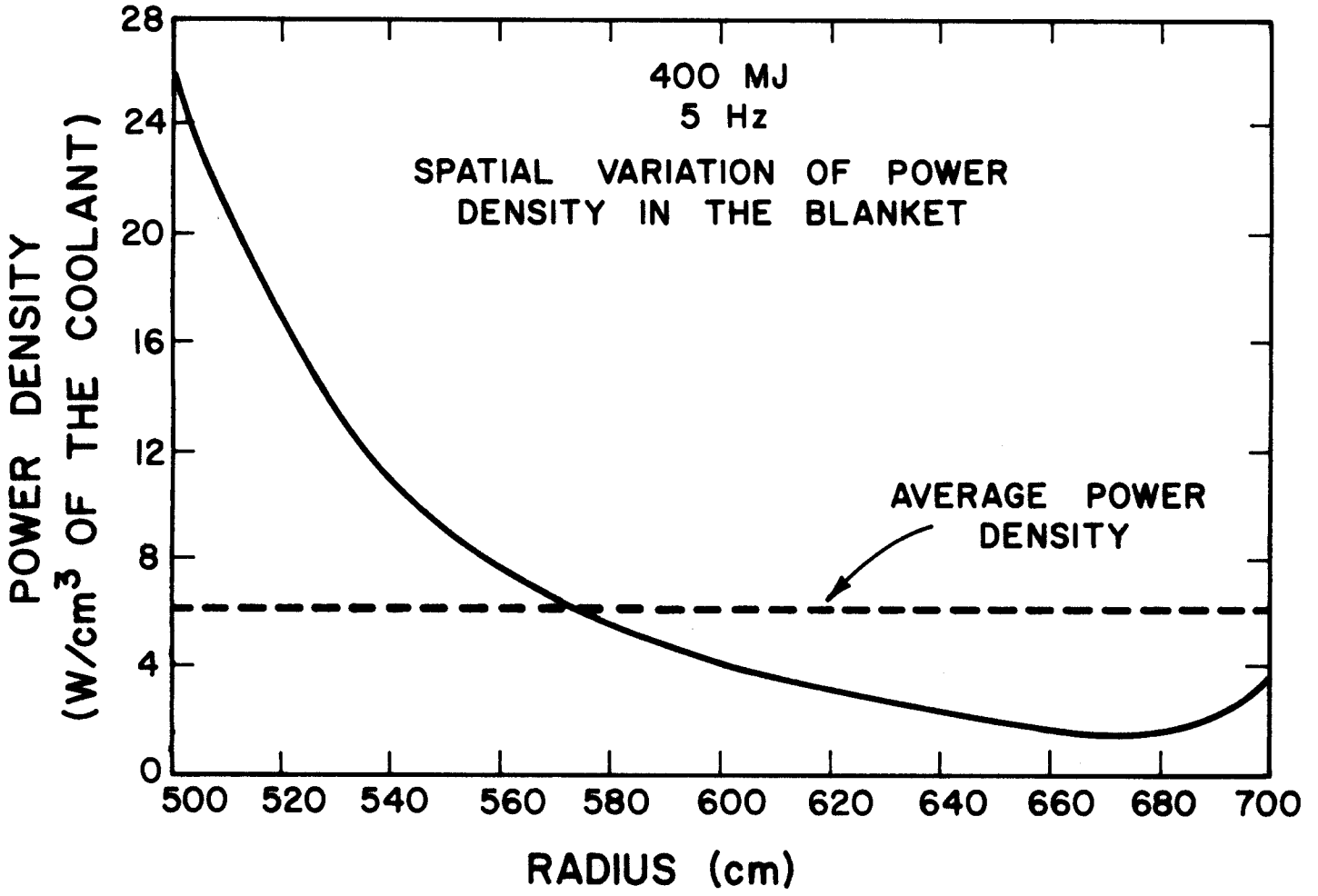

Figure 9 Spatial variation of power density in the blanket.

Table 8

Effect of Blanket Thickness and Target Interactions on Nuclear Energy Deposition (MeV/fusion)

		Neutron Target Interactions Included				14.1 MeV Source
Effective Blanket Thickness (cm)		0	25	50	60	60
Region						
Blanket	Neutrons	-	4.639	7.772	8.541	8.951
	Gamma	-	5.476	6.013	6.016	6.554
	Total	-	10.115	13.785	14.557	15.505
First Wall	Neutrons	.407	.071	.019	.011	.012
	Gamma	1.141	.412	.211	.153	.159
	Total	1.548	.483	.230	.164	.171
Reflector	Neutrons	2.626	.735	.235	.149	.157
	Gamma	14.402	7.473	3.232	2.197	2.295
	Total	17.028	8.208	3.467	2.346	2.452
Total		18.576	18.806	17.482	17.067	18.128
Overall Energy Mult.		1.326	1.340	1.264	1.240	1.229

of 14.1 MeV neutron source. As the blanket thickness increases, the total energy deposited in it increases with a larger fraction of this energy being deposited by neutrons. The larger energy deposition results from the larger number of neutron and gamma interactions taking place in the thicker blanket. The relative gamma contribution to the heating decreases as the thickness increases because a smaller portion of the blanket will be adjacent to the first wall where large gamma production occurs. The neutron and gamma heating in the first wall and reflector decrease as the blanket thickness increases because of the increased neutron attenuation in the blanket. The total energy deposited in the system is found to decrease as the blanket thickness increases. This results because of the decreased production in ferritic steel due to smaller neutron densities in the first wall and reflector. The energy multiplication is also included in Table 8. This factor is defined as the total energy deposited in the system, including the energy deposited by X-rays and pellet debris at the first surface of the blanket, divided by the fusion reaction yield of 17.6 MeV. The results of Table 8 show also that neglecting neutron target interactions tends to overestimate the neutron and gamma energy deposition in the blanket - reflector system.

The energy flow for the University of Wisconsin HIB fusion reactor design is illustrated in Fig. 10. The values given for the power correspond to the whole power plant with four reactor cavities.

VIII. Summary

Consistent coupled target - blanket neutronics and photonics calculations are performed for the University of Wisconsin heavy ion beam fusion reactor conceptual design. Neutron spectrum softening, neutron multiplication, and gamma production resulting from neutron target interactions are considered.

Figure 10

ENERGY FLOW IN THE REACTOR

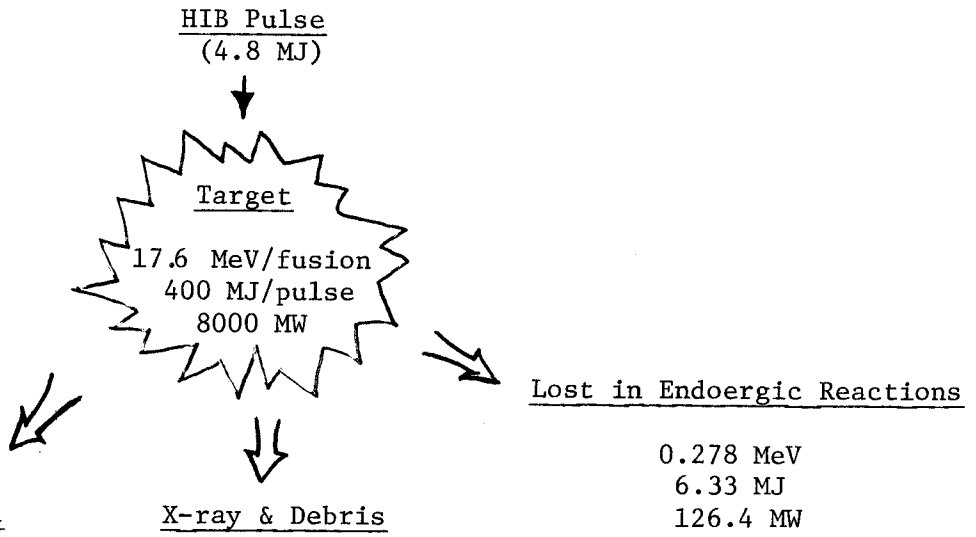

	Neutron & Gamma	X-ray & Debris	Total		
Cavity Region	14.56 MeV 330.91 MJ 6618.2 MW	4.763 MeV 108.25 MJ 2165 MW	19.323 MeV 439.16 MJ 8783.2 MW	(88.5%)	21.833 MeV 496.19 MJ 9925.1 MW
Wall	0.16 MeV 3.73 MJ 74.7 MW		0.16 MeV 3.73 MJ 74.7 MW	(0.75%)	
Reflector	2.35 MeV 53.3 MJ 1066.2 MW		2.35 MeV 53.3 MJ 1066.2 MW	(10.75%)	
Shield	0.515 MeV 1.17 MJ 23.4 MW	Leakage			

Overall energy multiplication = 1.2406

= 1.2436 (If leakage is absorbed in shield)

70.75% of the neutrons are found to escape from the target without any collision. Very little tritium production occurs in the target. A tritium breeding ratio of 1.175 is obtained. An overall energy multiplication of 1.24 is found to be achieved in the system.

Increasing the blanket effective thickness is found to increase tritium breeding, atomic displacement in SiC tubes, and energy deposition in the blanket. On the other hand, dpa rates in ferritic steel, gas production in SiC and ferritic steel, and total energy deposition are found to decrease as the blanket thickness increases.

Neglecting neutron target interactions is found to overestimate tritium production, dpa rate in ferritic steel, gas production in SiC and ferritic steel, and neutron and gamma heating, and to underestimate dpa rate in SiC.

Acknowledgement

Funding for this work was provided by the Kernforschungszentrum Karlsruhe, Federal Republic of Germany.

References

1. M. Ragheb, E. Cheng, and R. Conn, Atomkernenergie (ATKE), 31/4, 217 (1978).

2. M. Ragheb, M. Youssef, S. Abdel-Khalik, and C. Maynard, Trans. Am. Nucl. Soc., 30, 59 (1978).

3. L. Booth and L. Leonard, Trans. Am. Nucl. Soc., 34, 58 (1980).

4. J. Pendergrass, et al., Trans. Am. Nucl. Soc., 34, 40 (1980).

5. P. Finn, et al., Trans. Am. Nucl. Soc., 34, 55 (1980).

6. R. Bangerter and D. Meeker, LLL Report UCRL-50021-76, pp. 4-44 (1980).

7. RSIC Code Package CCC-254, "ANISN-ORNL," Radiation Shielding Information Center, ORNL.

8. RSIC Data Library Collection, "VITAMIN-C, 171 Neutron, 36 Gamma-Ray Group Cross Sections Library in AMPX Interface Format for Fusion Neutronics Studies," DLC-41, ORNL.

9. RSIC Data Library Collection, "MACKLIB-IV, 171 Neutron, 36 Gamma-Ray Group Kerma Factor Library," DLC-60, ORNL.